Received: 20 December 2023 | Revised: 19 March 2024 | Accepted: 19 March 2024

DOI: 10.1002/ar.25447

SPECIAL ISSUE ARTICLE

The Anatomical Record WILEY

Bending performance changes during prolonged canine eruption in saber-toothed carnivores: A case study of *Smilodon fatalis*

Z. Jack Tseng

Department of Integrative Biology and Museum of Paleontology, University of California, Berkeley, California, USA

Correspondence
Z. Jack Tseng, Department of Integrative Biology and Museum of Paleontology, University of California, Berkeley, CA 94720, USA.
Email: zjt@berkeley.edu

Funding information
National Science Foundation, Division of Biological Infrastructure, Grant/Award Number: 2128146

Abstract

The canine of saber-toothed predators represents one of the most specialized dental structures known. Hypotheses about the function of hypertrophied canines range from display and conspecific interaction, soft food processing, to active prey acquisition. Recent research on the ontogenetic timing of skull traits indicates the adult canine can take years to fully erupt, but the consequences of prolonged eruption on inferences of canine functional morphology are missing from current discourse and have not been quantified. Here I evaluate hypotheses about adult canine bending strength and stiffness, respectively, during eruption in the felid *Smilodon fatalis*. Simulated eruption sequences of three adult canines were generated from specimen models to assess shifting cross-sectional geometry properties, and bending strength and stiffness under laterally directed loads were estimated using finite element analysis. Consistent with beam theory expectations, *S. fatalis* canine cross-sectional geometry is optimized for increased bending strength with increased erupted height. However, canine cross-sectional geometry changes through eruption exaggerate rather than minimize lateral deflection. Spatial constraint for maximum root length from adjacent sensory structures in the maxilla and the recently identified universal power law are hypothesized to limit the growth capacity of canine anteroposterior length and, consequently, maintenance of bending stiffness through eruption. Instead, the joint presence of the deciduous and adult canines for >50% of the adult canine eruption period effectively increases canine mediolateral width and brings bending strength and stiffness estimates closer to theoretical optima. Similarly prolonged retention of deciduous

Abbreviations: AMNH FM, fossil mammals collection of the American Museum of Natural History Division of Paleontology; AP, anteroposterior; CT, computed tomography; δ_{ML}, mediolateral deflection of canine; *E*, elastic modulus; *F*, applied force; FE, finite element; *h*, canine height; I_{AP}, second moment of area around the anteroposterior axis; KU, Kansas University Natural History Museum; LACM RLB, Rancho la Brea collection of the Natural History Museum of Los Angeles County; ML, mediolateral; N, Newtons (measure of force); S_{AP}, Bending strength around anteroposterior axis; *x*, canine anteroposterior length; *y*, canine mediolateral width.

canines in other sabertooths suggests dual-canine buttressing is a convergently evolved strategy to maximize bending strength and stiffness.

KEYWORDS

beam theory, carnivore, convergent evolution, finite element analysis, functional morphology

1 | INTRODUCTION

Saber-like canine teeth evolved convergently in multiple vertebrate clades, including five times within mammals (Lautenschlager et al., 2020). Despite the ongoing debate regarding predatory behavior implied by the morphologically specialized canine teeth of saber-toothed predatory mammals (machairodontine felids, nimravids, barbourofelids, thylacosmilids, creodonts) (e.g., Andersson et al., 2011; Antón & Galobart, 1999; Anyonge, 1996; Biknevicius et al., 1996; Deng et al., 2016; Domínguez-Rodrigo et al., 2022; Emerson & Radinsky, 1980; Figueirido et al., 2018; Martin, 1980; McCall et al., 2003; Meachen-Samuels, 2012; Wroe et al., 2008, 2013), one consistent theme in sabertooth bite mechanics research is the emphasis on fully erupted adult (permanent) canines (Wysocki, 2019). Although fully adult canines represent the most impressive and oft-discussed versions of the elongate teeth, the observation that subadult individuals of the extinct felid *Smilodon fatalis* and other sabertooths spent a substantial amount of time living with partially erupted canines suggests that the months to years leading up to full adult canine eruption may be crucial ones for understanding sabertooth function in adult individuals. Wysocki et al. (2015) estimated that the maximum timespan required for adult canines to fully erupt in *S. fatalis* may have been just shy of 30 months. Thus, sub-adult sabertooths would have had to adjust to a continuously shifting set of dental weaponry for more than 2 years during their ontogeny. The importance of such acclimation to a shifting dentition is underscored by observations that *S. fatalis* from the Rancho La Brea Tar Pits exhibit higher incidents of tooth breakage than other commonly found predators in the region such as dire wolves (Binder & Van Valkenburgh, 2010; van Valkenburgh & Hertel, 1993).

The cross-sectional geometry of canine crowns has been shown to play an important part in determining the fracture resistance (Freeman & Lemen, 2007a; Soukup et al., 2015) as well as the functional specialization and ecological correlation (Freeman & Lemen, 2007b; Pollock, Hocking, & Evans, 2022; Pollock, Panagiotopoulou, et al., 2022) of canine teeth in extant carnivoran mammals. It has long been observed that the hypertrophied canines of sabertooth carnivorans such as *S. fatalis* exhibit varied cross-sectional geometry along the height axis of the tooth (Merriam & Stock, 1932; Tseng et al., 2010; Wysocki, 2019). However, the resulting changes in mechanical performance of the saber-like teeth through various stages of eruption have not been explicitly quantified.

Prior research on the functional morphology of sabertooth canines have firmly established the utility of beam theory in clarifying patterns of functional variation across adult canines of different sabertooth taxa (Christiansen, 2007; Van Valkenburgh & Ruff, 1987) as well as mandibles (Therrien, 2005). The bending strength of a beam-like canine structure around its anteroposterior axis (S_{AP}) is defined using beam theory as:

$$S_{AP} = \frac{I_{AP}}{hy}$$

where h is the canine height, y is the mediolateral width of the canine, and I_{AP} the second moment of area (a measure of how material is distributed in the cross-section of the beam-like structure) around the bending axis, defined as:

$$I_{AP} = \frac{\pi x y^3}{4}$$

where x is the anteroposterior length of the canine, and y as above. If we substitute the formula for second moment of area into the bending strength formula above, S_{AP} becomes:

$$S_{AP} = \frac{\pi x y^2}{4h}$$

Based on this equation, it is expected that for bending strength of saber-like canines that exhibit beam-like behavior to stay constant with increasing crown height, xy^2 should increase linearly with h. See Figure 1h for visual definitions of the terms used in the equation.

Furthermore, it can also be shown from beam theory principles that if both the load placed on a beam-like cantilever structure such as a sabertooth canine and its elastic modulus (a material property that describes stiffness)

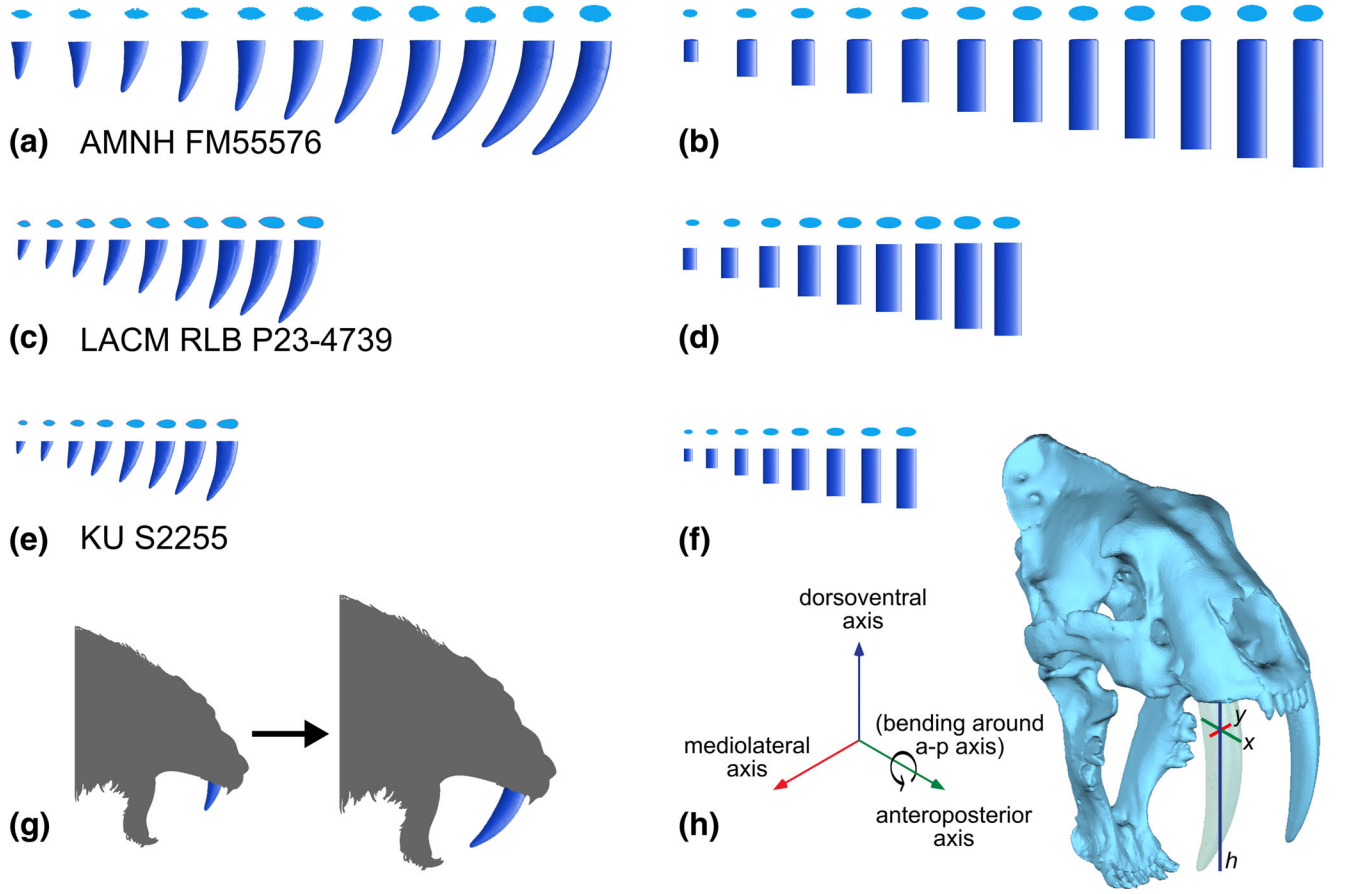

FIGURE 1 Canine eruption and beam models of *Smilodon fatalis* analyzed in the study. (a) Canine eruption sequence models based on AMNH FM55576, (b) Beam models based on AMNH FM55576, (c) Canine eruption sequence models based on LACM RLB P23-4739, d. Beam models based on LACM RLB P23-4739, (e) Canine eruption sequence models based on KU S2255, (f) Beam models based on KU S2255. (g) Approximate positions of two different canine eruption stages to demonstrate the eruption sequence tested in the study. Silhouette modified from phylopic.org (credit: Steven Traver, CC0 license). (h) The axis system, dimensional terms, and the specific mode of bending tested using beam theory equations in this study. Lighter blue outlines in panels (a–f) represent cross-sectional geometries; darker blue shapes represent lateral views of models. Canine model sizes are at the same scale, showing variation in the size and height of adult canines.

are assumed to stay the same, then the total mediolateral deflection (δ_{ML}, the weakest axis of the saber-like canines) of the canine from a given load would be proportional to:

$$\delta_{ML} \propto \frac{h^3}{I_{AP}} = \frac{h^3}{\frac{\pi x y^3}{4}} = \frac{4}{\pi} \times \frac{1}{x} \times \left(\frac{h}{y}\right)^3$$

Therefore, to keep deflection (which is inversely proportional to bending stiffness) of the canine about the anteroposterior axis constant, xy^3 should increase linearly with h^3. These two strength and deflection expectations are the minimum beam theory-based requirements for maintaining saber mechanical performance through the eruption period.

Given (1) the expected cross-sectional geometry changes predicted by the beam theory equations shown above, (2) the prior observation that fully erupted adult canines in *S. fatalis* tend to have higher bending strength than expected from estimated masticatory forces (Christiansen, 2007), and (3) the fact that laterally compressed canines such as those found in saber-toothed predators are mechanically weakest in the mediolateral bending direction, I hypothesize that *S. fatalis* exhibit increased canine mediolateral bending strength and maximum deflection (stiffness) changes through their prolonged eruption period in order to maintain, if not improve, sabertooth mechanical performance. Namely,

> **H1.** The eruption sequence of *S. fatalis* adult canines is characterized by the maintenance or an increase in bending strength, specifically by following a cross-sectional geometry where xy^2 increases linearly with regard to h, and/or.

H2. The eruption sequence of *S. fatalis* adult canines is characterized by the maintenance or a decrease in maximum deflection, specifically by following a cross-sectional geometry where xy^3 increases linearly with regard to h^3.

If both H1 and H2 are supported, it would suggest that the canine eruption period in *S. fatalis* was evolutionarily optimized for maintaining (or increasing) strength and stiffness throughout the ontogenetic transition towards fully erupted adult canine morphology. If only one of the hypotheses is supported, it would suggest that sabertooth canines were only partially optimized, for either strength or stiffness but not both. If neither hypothesis is supported by data, then it would suggest that sabertooth canines are not optimized for strength or stiffness during eruption, and that either the adult canines are minimally load-bearing relative to less erupted versions of themselves, and/or that there are musculoskeletal and/or behavioral mechanisms, extrinsic to canine morphology, for preventing high loads along the weakest, mediolateral axis of the saber-like teeth. I test these hypotheses using a combination of beam theory analysis and finite element simulations, which have been previously shown to capture broad patterns of canine functional morphology across mammalian carnivores (Pollock, Panagiotopoulou, et al., 2022).

2 | MATERIALS AND METHODS

Three isolated *S. fatalis* permanent (non-deciduous) canines were used to generate eruption sequences for modeling: a 3D model of AMNH (American Museum of Natural History) FM55576 from Tseng et al. (2016) (right canine), KU (Kansas University Natural History Museum) S2255 from morphosource.org (https://www.morphosource.org/concern/media/000007490) (right canine), and LACM (Natural History Museum of Los Angeles County) RLB P23-4739 (https://www.morphosource.org/concern/media/000454821) (left canine) from morphosource. All three specimens represent surface morphology only: the AMNH specimen is a 3D model built from a CT scan of a specimen cast, and the LACM and KU specimens are models made from 3D surface scans of original specimens.

The 3D canine models were imported into Geomagic Wrap (version 2020; 3D Systems, Rock Hill, South Carolina), where they were patched and smoothed to remove preservational artifacts (i.e., holes and cracks). The long axes of the canine models were then aligned with a global vertical axis. Next, the canines were digitally duplicated and then manually translated dorsally in the vertical axis by 10 mm intervals relative to a horizontal plane representing the hypothetical "gumline," followed by rotation around the mediolateral axis so that the mesial and distal edges of the new canine base were perpendicular relative to the horizontal plane (Figure S1). This operation is akin to simulating canine eruption in reverse. The process was repeated for the three canine models until the new erupted canine height was between 20 and 40 mm, at the crown height of typical extant felids. These digital operations resulted in a simulated eruption sequence of the canine models from ~20 mm to their full erupted height of 100–140 mm (Figure 1a,c,e). This simulated eruption sequence roughly corresponds to the maxillary growth stages 7–10 of Tejada-Flores and Shaw (1984); during these stages the cheek teeth finish their eruption (Stage 7), the deciduous canine is shed (Stage 9), and the jugo-squamosal and basioccipital-basisphenoid sutures fuse (Stage 10).

To evaluate the accuracy of beam theory-based models in replicating mechanical behavior of morphology-based models, a parallel set of digital models representing cantilever beams were constructed by generating cylindrical polygon meshes within Geomagic Wrap using the anteroposterior (AP) length, mediolateral (ML) width, and total cusp height of each model in the simulated eruption sequence as input dimensions (Figure 1b,d,f). The AP and ML dimensions of each eruption model were taken at the plane representing the alveolar margin (Figure S1, f). Both morphological (3D models built using the actual sabertooth models) and beam (cylindrical models built from length, width, and height dimensions only) models were then imported into Strand 7 R3.1.1 (Strand7 Pty Ltd, Sydney, Australia) finite element analysis software. The models were solid-meshed using four-noded tetrahedral elements using the "medium" mesh density setting. Given the objective of comparing relative performance through an eruption sequence based on the geometry of each model only, a single set of homogeneous material properties was assigned to all models in the eruption sequences; E, or elastic modulus, was set at 18 GPa, and Poisson ratio was set at 0.3 (Tseng et al., 2016).

I assigned identical boundary conditions to all models by fully constraining (i.e., no translational movement in x, y, or z axes) four nodes at the base of each model on its dorsal-facing face; additionally, a single, laterally-directed nodal force of 80 N (arbitrarily defined, based on preliminary analysis of 3D-printed resin models of the same canine specimens that exhibited fracture at 80 N [ZJT unpublished data]) was defined at the tip of each model (Figure S2). Nodal forces are placed on the labial side of tooth models (i.e., the force is direct lingually from the labial side) and an arbitrary side on beam models because the latter is completely symmetric in shape. Given the focus of this study on how the same tooth at different stages of eruption

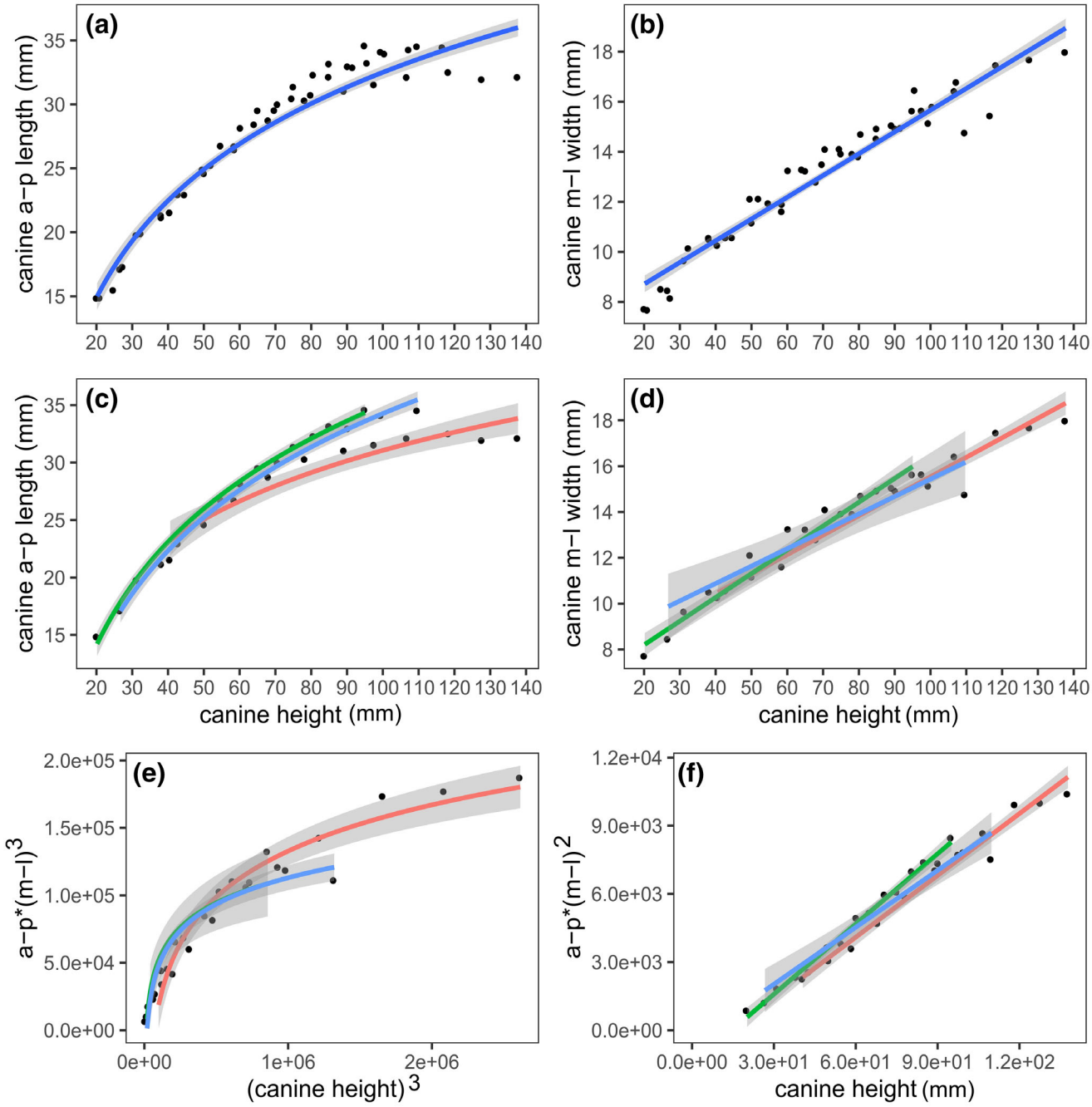

FIGURE 2 Changes in canine cross-sectional dimensions with height. (a) Canine height versus anteroposterior (a-p) length for both morphology and beam models, (b) Canine height versus mediolateral (m-l) width for both morphology and beam models, (c) Canine height versus a-p length for morphology models only, (d) Canin height versus m-l length for beam models only. (e) Relationship between height and cross-section geometry as terms in the beam deflection equation. (f) Relationship between height and cross-section geometry as terms in the beam strength equation. Solid lines (dark blue: all data; red: AMNH FM55576; light blue: LACM RLB P23-4739; green: KU S2255) represent the best fitted regression model and shading represents 95% confidence intervals.

deforms and resists the same bending force, tooth size and force were not further scaled (see Dumont et al., 2009 for a discussion of situations where scaling is necessary for FE output comparisons). The fully parameterized models were then solved using Strand7's linear static solver. To test the hypotheses stated in the introduction, two mechanical attributes were measured from each model: maximum displacement at the cusp tip (as a proxy for maximum deflection) in the direction of the force vector load at the node of the load, and 90th percentile maximum von Mises stress in a given model (as a proxy for bending strength). I chose a conservative cutoff of 10% for von Mises stress values,

TABLE 1 Canine morphological and mechanical performance regression statistics.

		All data		Morphology only		Beam theory only		Mean maximum Δ% through eruption	
Variables	**Model**	***F***	***p***	***F***	***p***	***F***	***p***	**Morphology**	**Beam theory**
Canine height ∼ canine a-p length	Log	641.60	<0.0001	259.80	<0.0001	383.40	<0.0001	195.33%	212.67%
Canine height ∼ canine w-l width	Linear	1048.00	<0.0001	451.10	<0.0001	571.70	<0.0001	185.33%	207.67%
Canine height^3 ∼ a-p × (m-l)^3	Log	2524.00	<0.0001	1107.00	<0.0001	1391.00	<0.0001	—	—
Canine height ∼ a-p × (m-l)^2	Linear	1626.00	<0.0001	748.00	<0.0001	832.60	<0.0001	—	—
Canine height ∼ bending displacement	Linear	14.99	0.003	12.28	0.001	18.95	0.0001	346.67%	422.67%
Canine height ∼ 90th percentile VM stress	Linear	12.00	0.001	78.45	<0.0001	15.74	0.0005	−162.00%	−208.33%

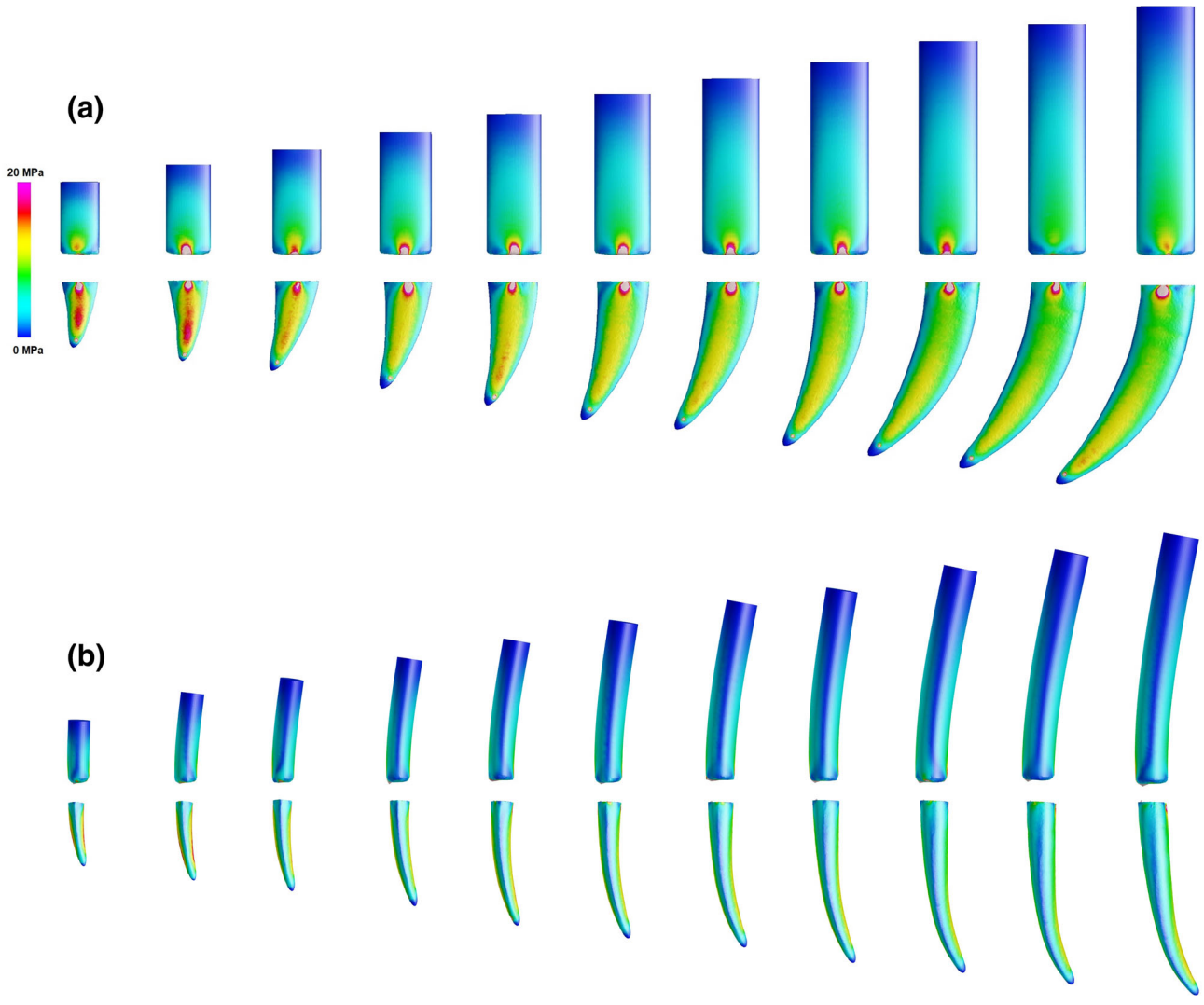

FIGURE 3 Finite element simulation of lateral bending in a canine eruption sequence. (a) Lateral view of models. (b) Anterior view of models. Heatmap shows von Mises stress values (in megapascal) for the eruption sequence beam models (top row in each panel) and morphology models (bottom row in each panel) based on AMNH FM55576. Anterior views represent a 10% deflection exaggeration to show relative deformations more clearly. Other models are not shown but they exhibit similar stress trends relative to canine eruption height.

rather than 2%–5% as done in some other studies (e.g., Marcé−Nogué et al., 2016; Walmsley et al., 2013), because only nodal forces and constraints (which create point-load and point-constraint artifacts in von Mises stress values in their immediate vicinity) were used rather than distributed surface loads. Furthermore, all model geometries were solid meshed at the same setting ("medium" mesh density), resulting in models containing between ~26,000 and ~500,000 tetrahedral elements according to physical size; thus, the smallest models contain larger number of elemental stress values under the influence of point-load artifacts than larger models. Therefore, I imposed the conservative cutoff of 10% of the highest von Mises stress values to mitigate these potential size biases. The displacement values measure the stiffness of a given model, and 90th percentile von Mises stress (excluding the point-load

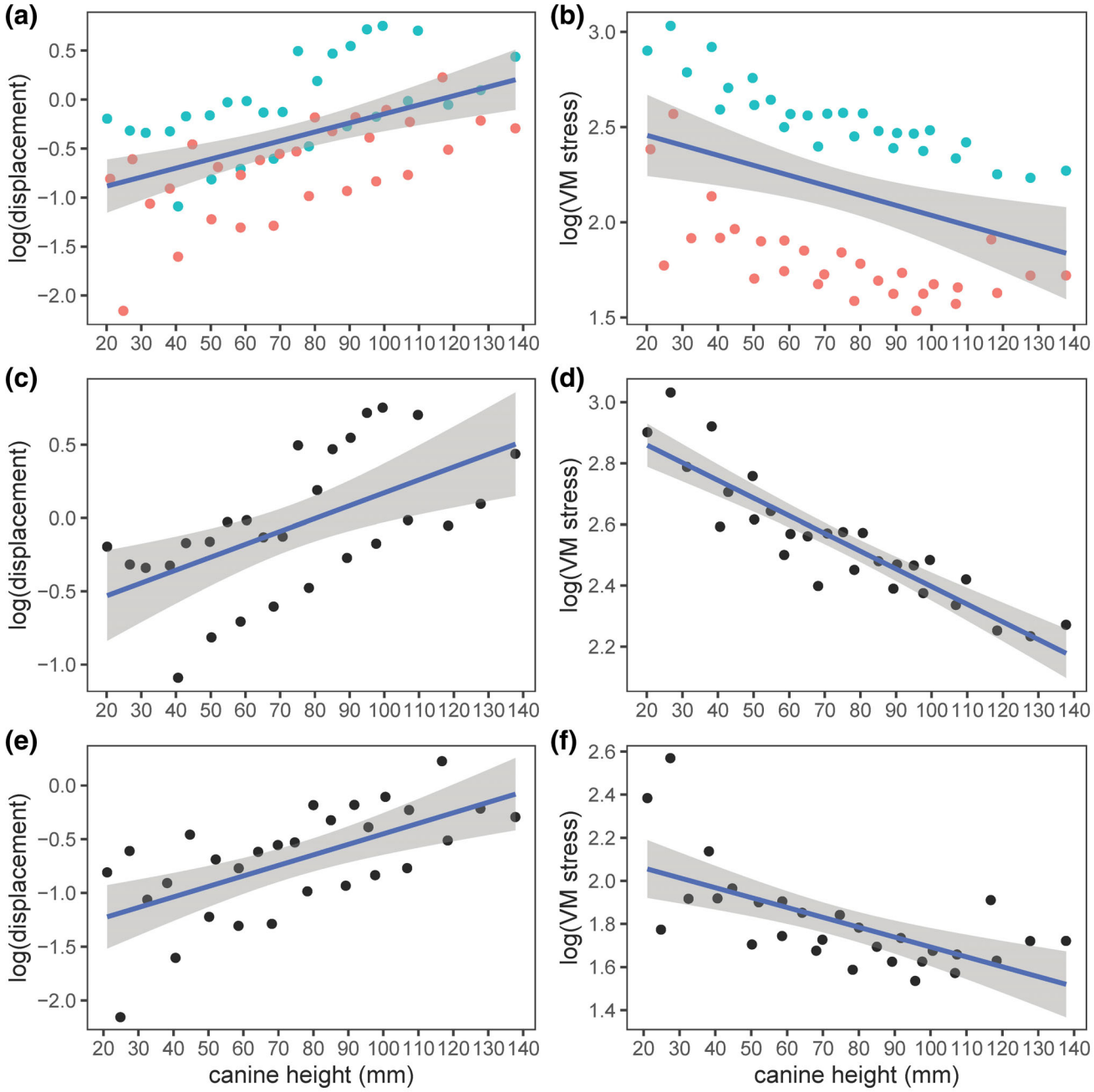

FIGURE 4 Relationship between canine eruption height and bending displacement and von Mises (VM) stress. (a) Canine height versus log bending displacement for all model data, (b) Canine height versus log VM stress for all model data, (c) Canine height versus log bending displacement for morphological model data only, (d) Canine height versus VM stress for morphological model data only, (e) Canine height versus log bending displacement for beam model data only, (f). Canine height versus VM stress for beam data only. Green circles in panels (a) and (b) represent morphological model data, red circles represent beam model data.

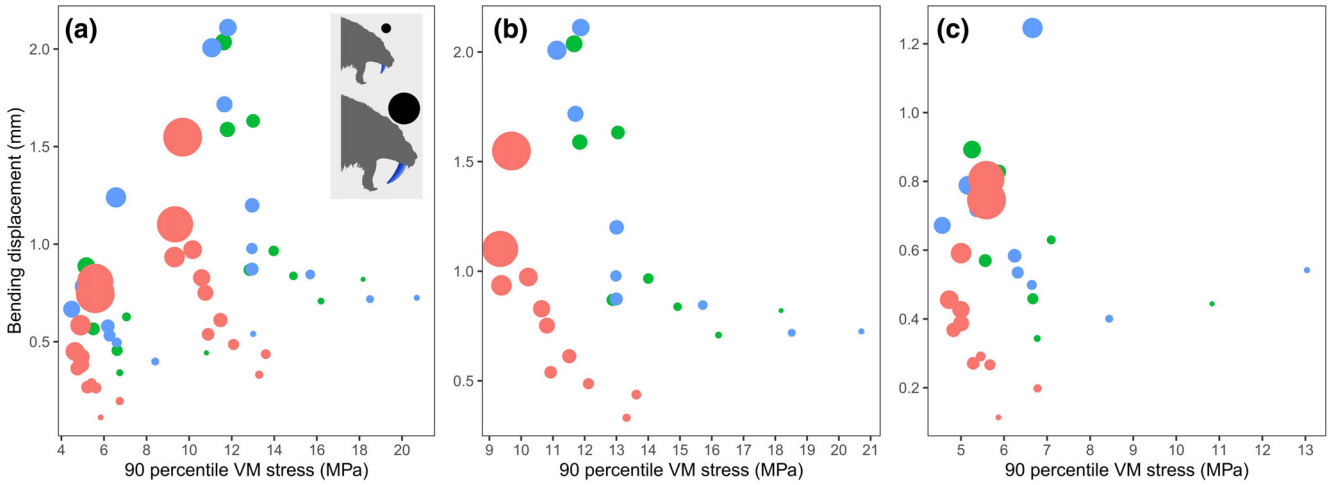

FIGURE 5 Relationship between simulated von Mises (VM) stress and bending displacement values through eruption. (a) All model data, (b) Morphological model data only, (c) Beam model data only. Note the inflection point for VM stress decrease occurs at lower erupted canine height than the inflection point for bending displacement increase. Red circles: AMNH FM55576; blue circles: LACM RLB P23-4739; green circles: KU S2255.

artifacts contained within the top 10% of the von Mises values, sensu Dumont et al., 2009) values measure the maximum strength of a given model.

To further assess the correlation between canine cross-section geometry, height, bending strength, and maximum deflection expected from beam theory, the relationships between simulation-derived performance measures and morphological dimensions of each model in the eruption sequences were modeled using regression analysis. The goodness of fit of the regression models were assessed using both the *F* statistic of the fitted model (amount of explained variance relative to unexplained variance) and its *p* value.

3 | RESULTS

The cross-sectional geometry of *S. fatalis* canines at the base of the crown follows a logarithmic trajectory of increase in the anteroposterior dimension and a linear trajectory of increase in the mediolateral dimension during eruption relative to height (Figure 2a–d). The three canine specimens exhibit minor variation in the shape of the fitted curve between canine height and cross-sectional geometry, but overall, the same trends are consistently observed across them. The relationship between the cross-sectional geometry terms and canine height in the bending strength equation is linear as hypothesized in H1 (that there should be maintenance or increase in bending strength with eruption; Figure 2f). The relationship between the cross-section geometry terms in the beam deflection equation and (canine height)^3 is logarithmic, contrary to the hypothesized linear trend in H2 (that there should be maintenance or a decrease in maximum deflection; Figure 2e). The *F* statistic and *p* values of the regression analyses are reported in Table 1. The full dataset is included in Table S1.

Early canine eruption stages exhibit higher von Mises stress concentrations on the lateral faces than later stages, as expected from the definition of mechanical stress (=force/area; the same force was applied to all models and later eruption stages have larger areas) (Figure 3). Accordingly, the 90th percentile maximum von Mises stress decreases with increasing canine eruption height (Figure 4b,d,f). The decrease in stress (and therefore increase in strength) is loglinear and consistent with H1. By contrast, the increase in maximum displacement at the cusp tip with increasing canine height (Figure 4a,c,e), suggests increased deflection with increasing canine height, contrary to expectations outlined in H2. In both stress and displacement values the change with canine height is best modeled by a logarithmic mode of change. Additionally, morphological models exhibit both higher displacement and higher stress compared to beam models (Figure 4).

The decrease in von Mises stress (i.e., increase in canine strength) with increasing canine height occurs earlier in the eruption sequence compared to the increase in displacement with increasing canine height (i.e., decrease in canine stiffness) (Figure 5). In other words, the erupting *S. fatalis* canine continues to exhibit increased deflection under the same lateral load even after it has reached its maximum strength at approximately 50–60% of the maximum canine height. Once again, beam models suggest a more rapid increase and higher maximum strength than the morphological models.

4 | DISCUSSION

The canines of saber-toothed predators such as *Smilodon fatalis* exhibit prolonged eruption periods relative to nonsaber-toothed mammals, even after accounting for elevated eruption rates (Feranec, 2004, 2008; Wysocki et al., 2015). I hypothesized that this prolonged transition to a fully adult state canine morphology followed a maintenance of lateral bending strength and deflection magnitudes in order to sustain saber mechanical performance through up to 30 months of canine morphological transition during eruption. Findings from canine cross-sectional geometry analysis indicate maintenance of a linear relationship between the cross-section and canine height terms of the beam theory bending strength equation (Figure 2b,d,f), and estimates of bending strength using finite element simulations in three eruption sequences suggest an increase in canine bending strength with increasing canine height (Figures 3 and 4b,d,f). These results support the predictions of H1, that the eruption sequence of *S. fatalis* adult canines is characterized by the maintenance or increase in bending strength.

In contrast, I found a logarithmic relationship between the cross-sectional geometry and crown height terms of the beam theory maximum mediolateral deflection equation, a pattern driven by a logarithmic increase in canine anteroposterior length relative to crown height (Figure 2a,c,e). Furthermore, maximum mediolateral displacement/deflection increases with canine height in both beam- and morphology-based finite element model simulations (Figure 4a,c,e). These findings are inconsistent with H2 predictions that the eruption sequence of *S. fatalis* adult canines is characterized by the maintenance or a decrease in maximum mediolateral deflection. Instead, maximum deflection increases (and therefore bending stiffness decreases) in lateral canine loading with increased erupted height. This pattern of increasing displacement is correlated with the fact that whereas canine mediolateral dimension changes linearly with regard to canine height, the increase in canine anteroposterior length increases slower at higher canine heights (Figure 2c,e). The slowdown of length increase in turn is associated with an acceleration of bending displacement/deflection later in the eruption sequence (Figures 3b and 5).

4.1 | Morphological limitations preventing minimized lateral deflection based on beam theory

The finding that canine mediolateral width increases linearly with regard to canine height allows further simplification of the beam theory mediolateral deflection equation and additional insights into potential limitations that prevent optimization of canine bending stiffness in *S. fatalis*. As alluded to in the introduction, the flexural rigidity equation for a cantilever beam defines maximum mediolateral deflection, δ_{ML}, under load F, as:

$$\delta_{ML} = \frac{Fh^3}{3EI_{AP}}$$

where h is the length of the beam (the crown height of the sabertooth canine), E is the elastic modulus of the tooth, and I_{AP} the second moment of area of the canine at its base. In the context of the finite element simulations conducted in this study, F (80 Newtons) and E (18 GPa) were defined as constant, therefore the maximum deflection of the canine (δ_{ML}) is proportional to:

$$\delta_{ML} \propto \frac{h^3}{I_{AP}} = \frac{h^3}{\frac{\pi x y^3}{4}} = \frac{4}{\pi} \times \frac{1}{x} \times \left(\frac{h}{y}\right)^3$$

Given the linear relationship observed between *Smilodon* canine height (h) and mediolateral width (y) from the analyses presented herein, the maximum lateral deflection given a load in the lateral direction can be further simplified and shown to be inversely proportional to canine anteroposterior length (x):

$$\delta \propto \frac{1}{x}$$

This suggests that to minimize lateral bending in the context of beam theory, selective pressure should favor sabertooth canines that exhibit linear or higher-power increase in x (anteroposterior length of canine; Figure 1h) with regard to increasing crown height. The finding that canine anteroposterior length increase is logarithmic rather than linear then begs an explanation of some constraint which prevents the linear relationship from being selected. Below I discuss anatomical, clade-specific, and universal factors that may contribute to such a pattern.

One possible morphological constraint that limits canine length increase could be the maximum canine growth volume in the maxillary bone of sabertooth carnivores. The maximum length of an adult *S. fatalis* canine is approximately equal to the maximum length of the anteroposterior space occupied by the canine root within the maxilla (for example, see specimen images in Merriam & Stock, 1932). The location of the canine root in between the nasal cavity and the infraorbital foramen may represent a spatial limitation, whereby canine size is

constrained by root chamber size, which is in turn limited by the necessary space for proper functioning of the adjacent olfactory system in the nasal cavity and the sensory system supplied by neurovascular bundles traveling through the enlarged infraorbital foramina. A similar interpretation has been made recently for the role of ever-growing canines in the South American marsupial sabertooth *Thylacosmilus* (Gaillard et al., 2023), and the presence of hypertrophied canines additionally has been cited as a potential factor in felid rostral skull shapes being exceptions to the general mammalian craniofacial allometry pattern (Tamagnini et al., 2023). More generally, the recently proposed power cascade model for elongate structures by Evans et al. (2021) suggests that unicuspid teeth represent power cone structures that follow a logarithmic spiral growth pattern. Thus, there may be universal as well as clade-specific anatomical factors that contribute to the sabertooth canine shape and exert control over its biomechanical limits. The fascinating possibility that the observed logarithmic increase in ML dimension in *Smilodon* canine along its height might reflect a universal logarithmic growth pattern of pointed teeth encourages further investigation.

4.2 | Possible evolutionary solutions to decrease lateral deflection during eruption

Wysocki et al. (2015) reconstructed the timing of major growth events in the skull of *S. fatalis* and showed that the deciduous canine may have remained in place during adult canine eruption for more than 50% of the total time required for the adult canine to fully erupt. From the perspective of beam theory, having both adult and deciduous canines side by side increases the effective mediolateral width of the canine complex (the permanent canine erupts lingually/medially to the deciduous canine; for some visual examples, see Tejada-Flores & Shaw, 1984). I conducted a post hoc analysis of such a configuration by adding 6 mm of ML width (based on observation and measurements of La Brea Tar Pits and Museum deciduous canine specimens HC-2001-9, HC-2001-75, HC-2001-104, HC-2003-R5, and A3509) to the ML width predicted by the regression model of height versus ML width in the actual fossil specimens used. I then recalculated the deciduous canine-reinforced bending strength and maximum deflection using beam theory. If such an additional width is incorporated into estimates of bending strength and maximum deflection, the offset in strength and deflection performance of a logarithmically increasing canine length would be alleviated by the reinforced canine width provided by the deciduous canines (Figure 6). The increase in total mediolateral width enabled by deciduous tooth buttressing brings beam theory estimates of bending strength and stiffness closer to the optimal trajectory predicted by a linear growth of cross-sectional geometry.

Permanent and deciduous canines in *Smilodon* exhibit different cross-sectional geometry that suggest different bending behavior through eruption; the permanent is relatively wider and more symmetrical in cross-section, whereas the deciduous is more extremely mediolaterally compressed and has a lingual groove that accommodates the space taken up by the erupting permanent canine. The biomechanical consequences of dual-canine buttressing may have favored heterochronic changes that prolonged the overlap between deciduous and permanent canine presence; the strengthening of the slender deciduous canine by the erupting permanent canine may have been as beneficial as the other way around. Future research could shed more light on the specific biomechanical changes progressing from the lone deciduous canine stage, to the dual-canine stage, and finally to the lone permanent canine stage and how those changes can be used to infer possible shifts in food acquisition and processing strategy.

Thus, the possible performance limitation imposed by root chamber size and universal growth patterns on maximum canine strength could be overcome by prolonging the duration of overlap between deciduous and adult canine *in situ*. Delayed deciduous canine eruption and shedding relative to deciduous cheek dentition has been observed not only in *S. fatalis* but also in other sabertooths such as barbourofelids, nimravids, and close relatives of *Smilodon* such as *Homotherium* (Bryant, 1988, 1990; Rawn-Schatzinger, 1983; Tseng et al., 2010; Wysocki, 2019), suggesting that this functional morphological solution to the problem of limited canine length growth may have convergently evolved in multiple sabertooth lineages (Wysocki, 2019). It is worth noting that at the end of the tooth replacement period, the fully erupted adult canine would still need to function alone, without contribution from a deciduous partner. Thus, bending stiffness would ultimately still experience a decrease relative to earlier eruption stages, and extrinsic means of controlling the magnitude of mediolateral loads on the tooth may be necessary to maximize the safety factor in lateral bending performance (see below).

4.3 | Additional considerations

Asymmetry in the cross-sectional shape of sabertooth canines, where the anteroposterior length is relatively larger than mediolateral width compared to extant felids, gives sabertooth felid canines their characteristic

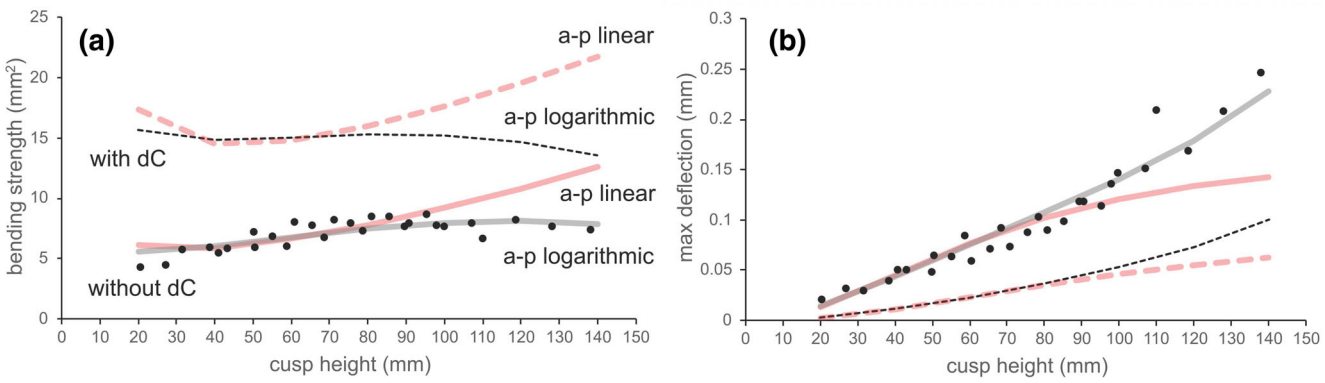

FIGURE 6 Beam theory-based predictions of optimization in saber bending mechanics. (a) Bending strength predictions; (b) maximum deflection (= maximum bending displacement at tip of cusp) predictions. Solid curves are predictions based on permanent canine eruption only; dotted curves are predictions based on contributions to effective mediolateral width from both permanent and deciduous (dC) canines during their overlapping eruption period. Gray curves represent logarithmic growth of canine anteroposterior (a-p) length (= observed in this study), red curves represent linear growth of a-p length (= hypothetical optimum). Black circles represent beam theory estimates based on actual cross-sectional geometry of specimens used in this study.

blade-like appearance. Although only mediolateral bending was tested in this study, the observed logarithmic growth of anteroposterior canine length rather than an optimized linear growth pattern also influences the progression of anteroposterior bending strength shifts under the beam theory framework. Anteroposterior bending strength estimates for different sabertooths are less variable than mediolateral bending strength values (Christiansen, 2007), but the extent to which factors discussed above for mediolateral bending also exert evolutionary limits on sabertooth canine strength and deflection evolution in anteroposterior bending would be worth further investigation.

The simulations conducted in this study assessed only a single laterally direct load at 80 N; however, prey-capture and food-processing forces most likely increased through ontogeny with enlarging body size and metabolic demands. If *S. fatalis* body mass growth rate was similar to extant lions, body mass increase over the period of canine eruption tested in this study would be equivalent to a 3–4 fold increase in body mass (Smuts et al., 1980). Additionally, adult *S. fatalis* exhibit cortical thickening in their humeri beyond what is observed in extant felids, suggesting a potentially important role of the forelimb in stabilizing the canine killing bite (Meachen-Samuels & Van Valkenburgh, 2010). The point at which an optimal linear anteroposterior length growth model diverges from the observe logarithmic growth model is around 80 mm in erupted canine height (Figure 6); this is at the upper end of the permanent canine erupted height range (65–80 mm) when Tejada-Flores and Shaw (1984) observed the loss of deciduous canine. The plateau in bending strength in the logarithmic growth model coinciding with dC loss further suggests that mechanisms extrinsic to the cross-section geometry of the canines may be responsible for controlling, if not minimizing, mediolateral deflection during predatory and/or agonistic behavior. The extent to which increased muscle forces and accompanied muscle control contribute to minimizing laterally directed forces on the adult canines would be interesting and important to quantify in future research.

5 | CONCLUSION

Beam theory-based assessment of bending strength and stiffness changes through the adult canine eruption sequence in *S. fatalis* demonstrates an optimal increase in canine width relative to height to provide bending strength increase. However, bending stiffness decreases as a result of limited, logarithmic increase in canine length, possibly due to spatial constraints in root size imposed by adjacent sensory structures in the maxilla and adherence to a universal power law for tooth growth. Nevertheless, the concomitant presence of the deciduous canine could have effectively overcome the compromised bending stiffness from the observed lag in canine length increase through eruption. Furthermore, increases in postcranial strength and overall body size and thus muscular strength and control through the ~30 months of adult canine eruption could have provided additional means of limiting laterally directed forces on the adult canines. These findings inform future hypothesis testing of sabertooth performance and behavior and especially encourage the treatment of hypertrophied canine functional morphology as a dynamic, rather than static, structural complex that captures evolutionary trade-offs between mechanical optimization and developmental constraint.

AUTHOR CONTRIBUTIONS

Z. Jack Tseng: Conceptualization; data curation; formal analysis; funding acquisition; investigation; methodology; project administration; resources; software; supervision; validation; visualization; writing – original draft; writing – review and editing.

ACKNOWLEDGMENTS

I would like to thank Juan Liu and members of the Functional Anatomy and Vertebrate Evolution Laboratory (both UC Berkeley) for their insightful discussion and suggestions during the earlier stages of this project. Thanks to Narimane Chatar for providing access to 3D models of *Smilodon* deciduous canines for the post hoc analysis. Many thanks to Doug Boyer and the morphosource.org team, and data managers Chris Widga and Aisling Farrell for making 3D data of the KU and LACM canine specimens used in this study openly downloadable. I thank Adam Hartstone-Rose, Tahlia Pollock, and Lars Werdelin for the invitation to participate in this special issue dedicated to the fascinating sabertooths, and AR editor Jeffrey Laitman for overseeing the issue. Finally, the three anonymous reviewers provided highly constructive and insightful comments that improved this manuscript. The study was supported in part by NSF DBI-2128146.

ORCID

Z. Jack Tseng https://orcid.org/0000-0001-5335-4230

REFERENCES

Andersson, K., Norman, D., & Werdelin, L. (2011). Sabretoothed carnivores and the killing of large prey. *PLoS One*, *6*(10), e24971. https://doi.org/10.1371/journal.pone.0024971

Antón, M., & Galobart, À. (1999). Neck function and predatory behavior in the scimitar toothed cat *Homotherium latidens* (Owen). *Journal of Vertebrate Paleontology*, *19*(4), 771–784. https://doi.org/10.1080/02724634.1999.10011190

Anyonge, W. (1996). Microwear on canines and killing behavior in large carnivores: Saber function in *Smilodon fatalis*. *Journal of Mammalogy*, *77*(4), 1059–1067. https://doi.org/10.2307/1382786

Biknevicius, A. R., van Valkenburgh, B., & Walker, J. (1996). Incisor size and shape: implications for feeding behaviors in sabertoothed "cats". *Journal of Vertebrate Paleontology*, *16*(3), 510–521. https://doi.org/10.1080/02724634.1996.10011336

Binder, W. J., & van Valkenburgh, B. (2010). A comparison of tooth wear and breakage in rancho La Brea sabertooth cats and dire wolves across time. *Journal of Vertebrate Paleontology*, *30*(1), 255–261. https://doi.org/10.1080/02724630903413016

Bryant, H. N. (1988). Delayed eruption of the deciduous upper canine in the sabertoothed carnivore *Barbourofelis lovei* (carnivora, Nimravidae). *Journal of Vertebrate Paleontology*, *8*(3), 295–306. https://doi.org/10.1080/02724634.1988.10011712

Bryant, H. N. (1990). Implications of the dental eruption sequence in Barbourofelis (carnivora, Nimravidae) for the function of upper canines and the duration of parental care in sabretoothed carnivores. *Journal of Zoology*, *222*(4), 585–590. https://doi.org/10.1111/j.1469-7998.1990.tb06015.x

Christiansen, P. (2007). Comparative bite forces and canine bending strength in feline and sabretooth felids: Implications for predatory ecology. *Zoological Journal of the Linnean Society*, *151*(2), 423–437. https://doi.org/10.1111/j.1096-3642.2007.00321.x

Deng, T., Tseng, Z., Hou, S.-K., & Zhang, Y.-X. (2016). A skull of *Machairodus horribilis* and new evidence for gigantism as a mode of mosaic evolution in machairodonts (Felidae, carnivora). *Vertebrata Palasiatica*, *54*(4), 302–318.

Domínguez-Rodrigo, M., Egeland, C. P., Cobo-Sánchez, L., Baquedano, E., & Hulbert, R. C. (2022). Sabertooth carcass consumption behavior and the dynamics of Pleistocene large carnivoran guilds. *Scientific Reports*, *12*(1), 6045. https://doi.org/10.1038/s41598-022-09480-7

Dumont, E. R., Grosse, I. R., & Slater, G. J. (2009). Requirements for comparing the performance of finite element models of biological structures. *Journal of Theoretical Biology*, *256*(1), 96–103.

Emerson, S. B., & Radinsky, L. (1980). Functional analysis of sabertooth cranial morphology. *Paleobiology*, *6*(3), 295–312. https://doi.org/10.1017/S0094837300006813

Evans, A. R., Pollock, T. I., Cleuren, S. G. C., Parker, W. M. G., Richards, H. L., Garland, K. L. S., Fitzgerald, E. M. G., Wilson, T. E., Hocking, D. P., & Adams, J. W. (2021). A universal power law for modelling the growth and form of teeth, claws, horns, thorns, beaks, and shells. *BMC Biology*, *19*(1), 58. https://doi.org/10.1186/s12915-021-00990-w

Feranec, R. S. (2004). Isotopic evidence of saber-tooth development, growth rate, and diet from the adult canine of *Smilodon fatalis* from rancho La Brea. *Palaeogeography, Palaeoclimatology, Palaeoecology*, *206*(3), 303–310. https://doi.org/10.1016/j.palaeo.2004.01.009

Feranec, R. S. (2008). Growth differences in the saber-tooth of three felid species. *PALAIOS*, *23*(8), 566–569. https://doi.org/10.2110/palo.2007.p07-079r

Figueirido, B., Lautenschlager, S., Pérez-Ramos, A., & van Valkenburgh, B. (2018). Distinct predatory behaviors in scimitar- and Dirk-toothed Sabertooth cats. *Current Biology*, *28*(20), 3260–3266.e3. https://doi.org/10.1016/j.cub.2018.08.012

Freeman, P. W., & Lemen, C. (2007a). An experimental approach to modeling the strength of canine teeth. *Journal of Zoology*, *271*(2), 162–169. https://doi.org/10.1111/j.1469-7998.2006.00194.x

Freeman, P. W., & Lemen, C. A. (2007b). The trade-off between tooth strength and tooth penetration: Predicting optimal shape of canine teeth. *Journal of Zoology*, *273*(3), 273–280. https://doi.org/10.1111/j.1469-7998.2007.00325.x

Gaillard, C., MacPhee, R. D. E., & Forasiepi, A. M. (2023). Seeing through the eyes of the sabertooth *Thylacosmilus atrox* (Metatheria, Sparassodonta). *Communications Biology*, *6*(1), 257. https://doi.org/10.1038/s42003-023-04624-5

Lautenschlager, S., Figueirido, B., Cashmore, D. D., Bendel, E.-M., & Stubbs, T. L. (2020). Morphological convergence obscures functional diversity in sabre-toothed carnivores. *Proceedings of the Royal Society B: Biological Sciences*, *287*(1935), 20201818. https://doi.org/10.1098/rspb.2020.1818

Marcé Nogué, J., de Esteban-Trivigno, S., Escrig Pérez, C., & Gil Espert, L. (2016). Accounting for differences in element size

and homogeneity when comparing finite element models: Armadillos as a case study. *Palaeontologia Electronica*, *19*, 1–22.

Martin, L. D. (1980). Functional morphology and the evolution of cats. *Transactions of the Nebraska Academy of Sciences and Affiliated Societies*, *287*(8), 141–154.

McCall, S., Naples, V., & Martin, L. (2003). Assessing behavior in extinct animals: Was Smilodon social? *Brain Behavior and Evolution*, *61*(3), 159–164. https://doi.org/10.1159/000069752

Meachen-Samuels, J. A. (2012). Morphological convergence of the prey-killing arsenal of sabertooth predators. *Paleobiology*, *38*(1), 1–14. https://doi.org/10.1666/10036.1

Meachen-Samuels, J. A., & van Valkenburgh, B. (2010). Radiographs reveal exceptional forelimb strength in the Sabertooth cat, Smilodon fatalis. *PLOS One*, *5*(7), e11412. https://doi.org/10.1371/journal.pone.0011412

Merriam, J. C., & Stock, C. (1932). *The Felidae of rancho La Brea*. Carnegie Institution of Washington Publication. https://search.proquest.com/docview/2356093328?accountid=14496

Pollock, T. I., Hocking, D. P., & Evans, A. R. (2022). The killer's toolkit: Remarkable adaptations in the canine teeth of mammalian carnivores. *Zoological Journal of the Linnean Society*, *196*(3), 1138–1155. https://doi.org/10.1093/zoolinnean/zlab064

Pollock, T. I., Panagiotopoulou, O., Hocking, D. P., & Evans, A. R. (2022). Taking a stab at modelling canine tooth biomechanics in mammalian carnivores with beam theory and finite-element analysis. *Royal Society Open Science*, *9*(10), 220701. https://doi.org/10.1098/rsos.220701

Rawn-Schatzinger, V. (1983). Development and eruption sequence of deciduous and permanent teeth in the saber-tooth cat Homotherium serum cope. *Journal of Vertebrate Paleontology*, *3*(1), 49–57. https://doi.org/10.1080/02724634.1983.10011958

Smuts, G. L., Robinson, G. A., & Whyte, I. J. (1980). Comparative growth of wild male and female lions (*Panthera leo*). *Journal of Zoology*, *190*(3), 365–373. https://doi.org/10.1111/j.1469-7998.1980.tb01433.x

Soukup, J. W., Collins, C., & Ploeg, H.-L. (2015). The influence of crown height to diameter ratio on the force to fracture of canine teeth in dogs. *Journal of Veterinary Dentistry*, *32*(3), 155–163. https://doi.org/10.1177/089875641503200302

Tamagnini, D., Michaud, M., Meloro, C., Raia, P., Soibelzon, L., Tambusso, P. S., Varela, L., & Maiorano, L. (2023). Conical and sabertoothed cats as an exception to craniofacial evolutionary allometry. *Scientific Reports*, *13*(1), 13571. https://doi.org/10.1038/s41598-023-40677-6

Tejada-Flores, A. E., & Shaw, C. A. (1984). Tooth replacement and skull growth in Smilodon from rancho La Brea. *Journal of Vertebrate Paleontology*, *4*(1), 114–121. https://doi.org/10.1080/02724634.1984.10011991

Therrien, F. (2005). Feeding behaviour and bite force of sabretoothed predators. *Zoological Journal of the Linnean Society*, *145*(3), 393–426. https://doi.org/10.1111/j.1096-3642.2005.00194.x

Tseng, Z., Takeuchi, G. T., & Wang, X. (2010). Discovery of the upper dentition of *Barbourofelis whitfordi* (Nimravidae, carnivora) and an evaluation of the genus in California. *Journal of Vertebrate Paleontology*, *30*(1), 244–254. https://doi.org/10.1080/02724630903416001

Tseng, Z. J., Grohé, C., & Flynn, J. J. (2016). A unique feeding strategy of the extinct marine mammal Kolponomos: Convergence on sabretooths and sea otters. *Proceedings of the Royal Society B: Biological Sciences*, *283*(1826), 20160044. https://doi.org/10.1098/rspb.2016.0044

van Valkenburgh, B., & Hertel, F. (1993). Tough times at La Brea: Tooth breakage in large carnivores of the late Pleistocene. *Science*, *261*(5120), 456–459. https://doi.org/10.1126/science.261.5120.456

van Valkenburgh, B., & Ruff, C. B. (1987). Canine tooth strength and killing behaviour in large carnivores. *Journal of Zoology*, *212*(3), 379–397.

Walmsley, C. W., Smits, P. D., Quayle, M. R., McCurry, M. R., Richards, H. S., Oldfield, C. C., Wroe, S., Clausen, P. D., & McHenry, C. R. (2013). Why the long face? The mechanics of mandibular symphysis proportions in crocodiles. *PLoS One*, *8*(1), e53873. https://doi.org/10.1371/journal.pone.0053873

Wroe, S., Chamoli, U., Parr, W. C. H., Clausen, P., Ridgely, R., & Witmer, L. (2013). Comparative biomechanical modeling of Metatherian and placental saber-Tooths: A different kind of bite for an extreme pouched predator. *PLoS One*, *8*(6), e66888. https://doi.org/10.1371/journal.pone.0066888

Wroe, S., Lowry, M. B., & Antón, M. (2008). How to build a mammalian super-predator. *Zoology*, *111*(3), 196–203. https://doi.org/10.1016/j.zool.2007.07.008

Wysocki, M. (2019). Fossil evidence of evolutionary convergence in juvenile dental morphology and upper canine replacement in sabertooth carnivores. *Ecology and Evolution*, *9*(22), 12649–12657. https://doi.org/10.1002/ece3.5732

Wysocki, M. A., Feranec, R. S., Tseng, Z. J., & Bjornsson, C. S. (2015). Using a novel absolute ontogenetic age determination technique to calculate the timing of tooth eruption in the saber-toothed cat, *Smilodon fatalis*. *PLOS One*, *10*(7), e0129847. https://doi.org/10.1371/journal.pone.0129847

SUPPORTING INFORMATION

Additional supporting information can be found online in the Supporting Information section at the end of this article.

How to cite this article: Tseng, Z. J. (2024). Bending performance changes during prolonged canine eruption in saber-toothed carnivores: A case study of *Smilodon fatalis*. *The Anatomical Record*, 1–13. https://doi.org/10.1002/ar.25447